Journal of
Synchrotron Radiation

ISSN 0909-0495

Received 16 January 2009
Accepted 2 July 2009

Soft X-ray characterization technique for Li batteries under operating conditions

Cole F. Petersburg,[a] Robert C. Daniel,[a] Cherno Jaye,[b] Daniel A. Fischer[b] and Faisal M. Alamgir[a]*

[a]School of Materials Science and Engineering, Georgia Institute of Technology, Atlanta, GA 30332, USA, and [b]Ceramics Division, National Institute of Standards and Technology, Gaithersburg, MD 20899, USA. E-mail: faisal.alamgir@mse.gatech.edu

O *K*-edge and Co *L*-edge near-edge X-ray absorption fine structure has been used to examine the cathode of an intact solid-state lithium ion battery. The novel technique allowed for the simultaneous acquisition of partial electron yield and fluorescence yield data during the first charge cycle of a $LiCoO_2$-based battery below the intercalation voltage. The chemical environments of oxygen and cobalt at the surface are shown to differ chemically from those in the bulk. The present design enables a wide variety of *in situ* spectroscopies, microscopies and scattering techniques.

Keywords: NEXAFS; XANES; Li ion battery; *in situ*; $LiCoO_2$.

1. Introduction

The excellent energy density (Tarascon & Armand, 2001) of rechargeable lithium batteries make them the preeminent energy storage technology for portable electronics and electric vehicles. Still, the safety and cycle life of intercalation cathodes are in doubt. Without direct measurements of the intercalation reaction as a function of cell potential over multiple cycles, selection of the best cathode material is guesswork. While it is known that a lithium ion leaving the cathode, upon charging, must be balanced by the loss of an electron, it is not known whether this electron comes from the transition metal ion alone or also from oxygen. Even for the dominant commercial cathode material, $LiCoO_2$, it is not clear whether the electron is taken from cobalt to form a Co^{4+} ion or from oxygen to produce O^- ions or oxygen gas (Dahn *et al.*, 1994). Although Co^{4+} has been detected by electron paramagnetic resonance in coordination complexes (Koikawa *et al.*, 1989), Co(IV) compounds are quite rare in nature and therefore may be highly reactive in a charged lithium battery. For mixed transition metal oxides, the picture is even more complex and interesting because multiple 3*d* metals with multiple oxidation states are reacting simultaneously, and influencing each other (Deb *et al.*, 2004). Any additional electron donation by oxygen ions would result in highly reactive species which may encourage the gradual combustion, or the violent explosion, of nonaqueous electrolytes. A method for detecting gas evolution and measuring the oxidation state of oxygen and the 3*d* transition metals *in situ* is presented.

Battery researchers have long sought to characterize cathode materials with X-rays *in situ* rather than *ex situ* because the requisite disassembly and washing of a cathode may change the bulk or surface composition significantly and eliminate internal electric fields. Furthermore, only one sample need be prepared to characterize an intercalation cathode at multiple cell potentials which not only reduces the work required but also eliminates variations owing to sample preparation. *Ex situ* methods become cumbersome when investigating the effects of multiple cycles. Only *in situ* cells can be measured over multiple cycles, enabling life cycle studies of cathodes. Extensive *in situ* X-ray absorption near-edge spectroscopy (XANES) work has successfully characterized these materials at the metal *K*-edges using hard X-ray energies above 4 keV with the use of Kapton windows and standard nonaqueous electrolytes. With this method, the oxidation states of transition metal ions in intercalation cathodes have been characterized as a function of state-of-charge (Deb *et al.*, 2004; Alamgir *et al.*, 2005). In these studies, a shift in the XANES spectra to higher energies is attributed partly to an increase in the 1*s* binding energy owing to a loss of 3*d* electrons which would otherwise shield the nucleus. As an alternative to XANES, one can measure the near-edge structure in electron energy loss spectroscopy (EELS), but EELS requires vacuum for both source and signal and has inferior signal quality compared with XANES for the analysis of 3*d* transition metals (Alamgir *et al.*, 2001).

Unfortunately, the dipole selection rule allows only $1s \rightarrow 4p$ transitions at the *K*-edge. The occupancy, configurations and energies of the 3*d* orbitals of the first-row transition metals, which form bonds with O in most Li battery cathodes, are not measured. The *L*-edge spectra, by contrast, arise due to $2p \rightarrow 3d$ transitions. The amplitudes of some near-edge features are

proportional to the number of empty 3*d* states, while changes in the 2*p* binding energy still cause energy shifts in the spectra. *In situ* XANES (called NEXAFS, near-edge X-ray absorption fine structure in the soft-X-ray context) of transition metal *L*-edges can provide more direct oxidation information than can *K*-edge XANES. In addition, hard X-ray *in situ* studies are seldom surface sensitive; the present method can show surface-to-bulk differences at the metal *L*-edges that could not be seen at the *K*-edges.

Additionally, soft X-ray NEXAFS spectroscopy accesses the $1s \rightarrow 2p$ transitions of lighter elements including C, O, S and P. The loss of O 2*p* electrons on deintercalation has been speculated to contribute to the capacity of $LiCoO_2$ (Montoro *et al.*, 2000; Yoon *et al.*, 2002; Alamgir *et al.*, 2005). Theoretical calculations (Ceder *et al.*, 1998) and hard X-ray EXAFS experiments (Alamgir *et al.*, 2005) suggest that oxygen contributes some of the capacity of $LiCoO_2$, possibly by forming O^- ions during the deintercalation of lithium. Also, the irreversible formation of Li_2O can be detected by its characteristic absorption spectrum. NEXAFS at the O *K*-edge, therefore, provides a great deal of information on intercalation reactions. Many *ex situ* studies (Montoro *et al.*, 2000; Uchimoto *et al.*, 2001; Yoon *et al.*, 2002) have shown $LiCoO_2$ and other cathodes at multiple states of charge by chemically or electrochemically adjusting the lithium content. Changes in both the oxygen *K*-edge and transition metal *L*-edges have been detected as a function of lithium content, but without the electric fields of a battery. These studies have been unable to show oxygen's *K*-edge spectrum in an assembled battery owing to design difficulties. X-rays below 1 keV in energy have attenuation lengths of $\sim$500 nm in solid materials; such a thin X-ray window cannot contain the pressure of a liquid electrolyte. Instead, a vacuum-compatible cell is required.

Only an *in situ* soft X-ray electrochemical cell, lacking windows or liquids, allows for surface-sensitive and bulk-sensitive spectroscopy over a continuous range of cell voltages and at multiple cycles. Recent advances in X-ray focusing can even enable spectromicroscopy at solid electrochemical interfaces on the top surface and along the outer profile of the cell. The exposure of the cell to vacuum allows mass spectroscopic methods and gas-exposure experiments. For example, the effect of water vapor and oxygen on the electronic structure of the cathode and anode at various voltages can be studied in such a packaging-free cell by adjusting the partial pressures of these gases in the vacuum chamber.

In the present study, surface-sensitive and bulk-sensitive NEXAFS measurements of the cathode of an intact packaging-free solid-state lithium battery are presented. Partial electron yield and fluorescence yield techniques reveal that the chemical environments of oxygen and of cobalt at the surface differ from those in the bulk in $LiCoO_2$. The cell was successfully charged in a vacuum synchrotron endstation under high vacuum conditions with simultaneous collection of surface-sensitive and bulk-sensitive signals. This is the first-ever reported *in situ* soft X-ray absorption study of a working lithium battery.

2. Experiment

2.1. Cell design and assembly

The experimental approach consists of a specially designed battery installed in a simple fixture. Because the battery consists entirely of solid materials, it has low vapor pressure and requires no windows. The conductive additives in the composite cathode, described below, allow current to flow easily to and from the cathode ($LiCoO_2$) particles without the need for a thin film current collector. The fixture merely provides electrical contacts. Importantly, any desired cathode or anode material can be used to construct the battery. The cathode, anode and electrode–electrolyte interfaces can be exposed to an incident beam of photons or electrons. The solid-state lithium battery consisted of a three-layer powder compact. The cathode layer consisted of a mixture of 14 wt% $LiCoO_2$ (7–10 µm, Sigma-Aldrich), 41 wt% solid electrolyte powder and 45 wt% acetylene black (Sigma-Aldrich) mixed in a SPEX 8000 planetary ball mill (without grinding media). The electrolyte layer consisted of partially amorphized lithium phosphorous sulfide glass of formula $60Li_2S{\cdot}40P_2S_5$. The electrolyte was mixed in an argon-filled glovebox, vacuum sealed into an agate vial equipped with Viton O-rings and three 12 mm agate balls, and amorphized in a SPEX 8000 mill for 20 h. X-ray diffraction showed the powder to contain a large amorphous fraction, indicating its lithium ion conductivity (Hayashi *et al.*, 2001). The cathode and electrolyte layers were pressed in a 13 mm die at 2050 kg cm^{-2} in an argon-filled glovebox containing less than 1 p.p.m. of moisture. A reference pellet consisting of as-received 95 wt% $LiCoO_2$ and 5 wt% PVDF was used for comparison.

The fixture providing electrical contact consists of a metal backplate in contact with an 11 mm disc of scraped lithium foil which in turn contacts the electrolyte-and-cathode pellet. The 4 mm-thick front plate contained an 8 mm hole for the benefit of spectroscopic experiments. The pellet side contained a shallow counterbore to hold the pellet in place. On the incident beam side, a 45° countersink allowed for wide collection angles. Nylon screws held the current collector plates together. Only double-sided conductive tape was required to affix the reference sample. Fig. 1(*a*) shows a schematic of the profile of this assembly together with a schematic of the profile of the three-layer battery. Fig. 1(*b*) shows a three-dimensional rendition of the assembly as well as a photograph of the actual assembly. The assembly was inserted into the loadlock of the analysis chamber at beamline U7A *via* a nitrogen-filled glovebag.

2.2. Electrochemical cycling

The battery was transferred from the loadlock to the soft X-ray analysis chamber and pumped down to 3×10^{-8} torr. It was charged *via* a feedthrough by a Solartron 1287 potentiostat. The initial voltage of the as-prepared battery was 1.9 V. It was later charged at 10 µA to 2.5 V for 10.5 h, followed by a second charging to 3.15 V at 25 µA for 5 h. At all times the battery remained below the onset voltage of approximately 3.9 V (Alamgir *et al.*, 2005).

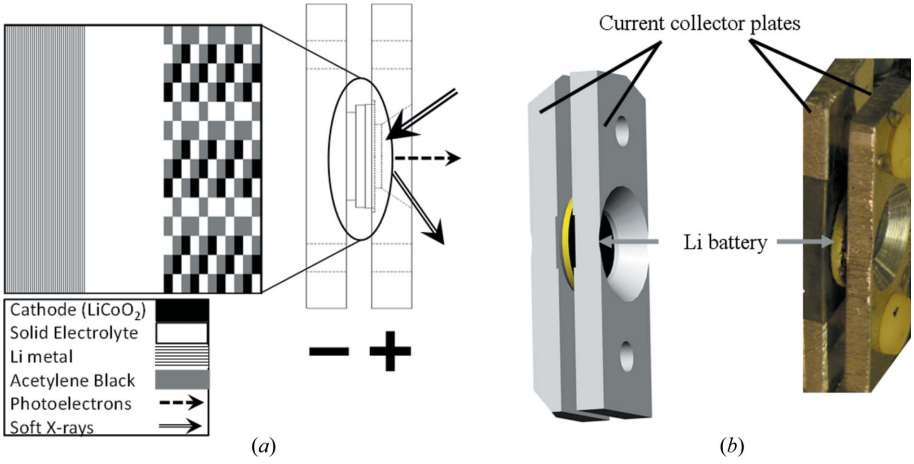

Figure 1
(*a*) Schematic cross-section view of the sample holder and an enlarged cutaway of the composite solid-state battery, including a lithium metal anode, a solid electrolyte layer, and a composite cathode composed of $LiCoO_2$, acetylene black and solid electrolyte. (*b*) Three-dimensional rendering of the cell assembly and a photograph of the actual assembly.

2.3. X-ray absorption measurements

NEXAFS spectra were recorded at the NIST soft X-ray beamline U7A of the National Synchrotron Light Source at Brookhaven National Laboratory. The incident beam irradiated the sample at 38° from the sample normal. Data were simultaneously collected in 0.2 eV steps from a partial electron yield (PEY) detector, held 35° above the sample normal, and from a fluorescence yield detector positioned perpendicular to the incident beam, or 52° from the sample normal. The PEY detector was biased at −250 V to reject low-energy electrons. The fluorescence yield (FY) data were filtered to include only O *K*-edge transitions, or only the fluorescence from cobalt in Co *L*-edge spectra. A clean high-transmittance gold mesh was used to calibrate the oxygen spectra and to normalize spectral intensity while an FeNiCrCo alloy mesh was used to calibrate cobalt spectra.

3. Results

NEXAFS spectra at the O *K*-edge in Fig. 2(*a*), in both PEY and FY modes, show a sharp resonance at 530 eV and broad pair of resonances around 540 eV with a shoulder feature at ∼535 eV. Relative to the PEY spectrum, the FY spectrum contains a more intense 530 eV resonance and a stronger 540 eV resonance. The shoulder resonance at 535 eV is lower in energy in the bulk-sensitive FY spectrum than in the PEY spectrum.

Co *L*-edge spectra in Fig. 2(*b*) show more dramatic peak height differences between the surface-sensitive PEY data and the bulk-sensitive FY data. In the geometry of our experiment, with the incident beam at the magic angle with respect to the sample surface, it is very easy to see that FY will be much more bulk sensitive than PEY at the O *K*- and Co *L*-edge in our sample. Because the incident beam entered the sample at 38° from the sample normal, fluorescence photons were both generated in and were able to escape from the bulk of the sample. Using a density of 5.16 g cc^{-1} for $LiCoO_2$ (Johnston *et al.*, 1958) and using calculations presented by Henke *et al.* (1993), the attenuation lengths of 543 eV incident photons and 525 eV exiting fluorescence photons travelling through $LiCoO_2$ are approximately 200 nm and 550 nm, respectively. Using the geometry of the measurements at the magic angle, the attenuation length of the incident photons is closer to 125 nm. In comparison, the Auger electrons in PEY have an inelastic mean free path of 2.5 nm in $LiCoO_2$ according to the model of Seah & Dench (1979) for similar incident energies. In other words, the information depth of fluorescence photons should be 50 times higher than that for PEY electrons for

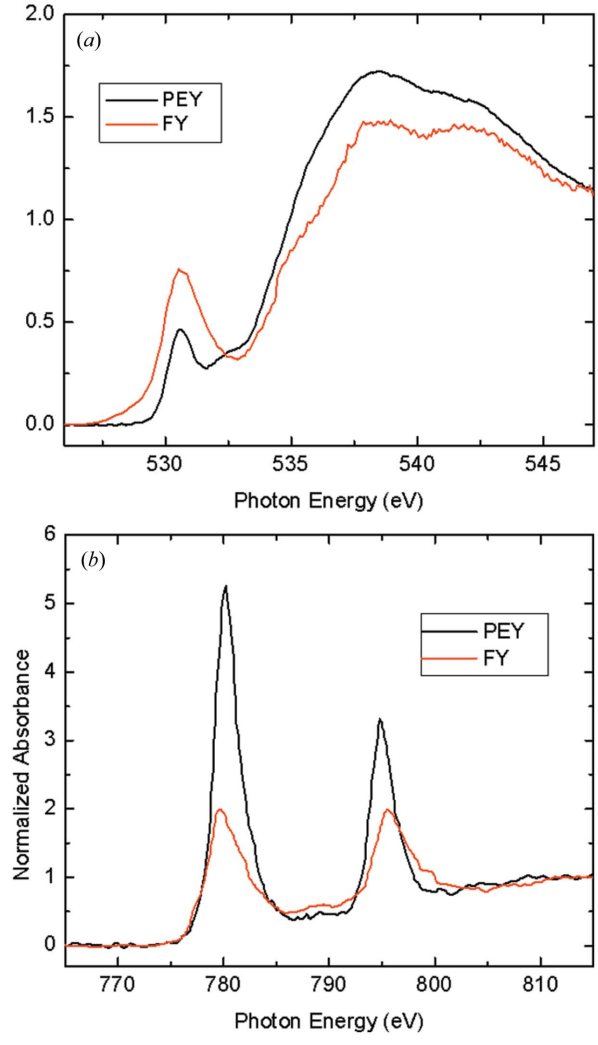

Figure 2
Comparison of normalized fluorescence yield (FY) and partial electron yield (PEY) NEXAFS spectra of $LiCoO_2$ at the (*a*) O *K*-edge, 3.1 V, and (*b*) Co *L*-edge, 2.5 V.

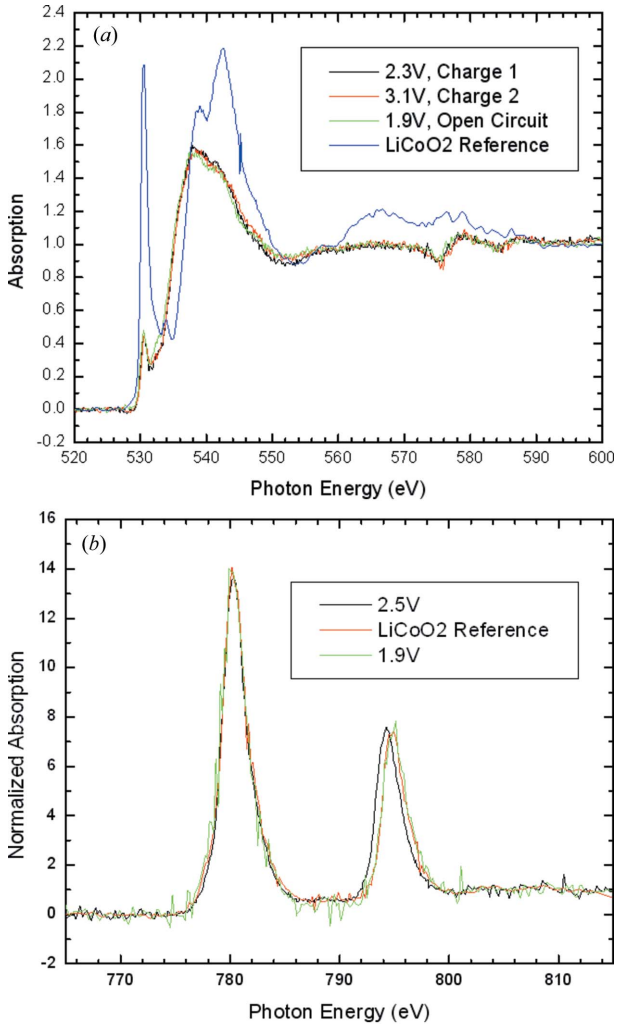

Figure 3
Partial electron yield NEXAFS (*a*) at the O *K*-edge at 1.9 V (open circuit), 2.3 V (current flowing) and 3.1 V (current flowing) as well as of reference $LiCoO_2$ (pressed with 5 wt% PVDF binder), and (*b*) at the Co *L*-edge at 1.9 V, at 2.5 V and of the same reference $LiCoO_2$ mentioned in (*a*).

our measurement conditions. The peak area ratios (L_3 *versus* L_2) in Fig. 2(*b*) differ; PEY scans show the 2:1 area ratio, which was expected based on spin considerations (Leapman *et al.*, 1982), while FY scans indicate a 1.5:1 ratio.

Fig. 3 compares the $LiCoO_2$ reference spectrum with the battery at three states of charge. At two of these states of charge the spectrum was recorded while a charging current was flowing. The spectrum of the battery is dramatically different from the reference sample spectrum. While the prepeak energy has not changed (after calibrating the spectra relative to the gold mesh spectra), the remaining features are at lower energies. The prepeak intensity is markedly lower in the battery compared with the reference sample, while the higher-energy features are slightly less intense.

In Fig. 3(*a*) a small feature between the prepeak and the pair of higher-energy peaks is shown. This feature is seen in the reference sample and at 1.9 V, but not at 2.3 V or 3.1 V in which cases current was flowing. Fig. 3(*b*) compares the PEY spectrum at the Co *L*-edge of the reference spectrum with that of the battery below the intercalation voltage. No significant changes are seen.

4. Discussion

The present design will allow for extensive *in situ* studies at higher voltages and over the course of many cycles. However, the present samples utilized an incompletely amorphized solid electrolyte, leading to a very high internal resistance in the cell. Together with an imperfect electrolyte–lithium-metal interface, the poorly amorphized solid electrolyte limited the speed of operation of the battery. In the best case, the sulfide electrolyte conductivity has been reported to reach 2.0×10^{-4} S cm^{-1} at 75% Li_2S/25% P_2S_5 (Hayashi *et al.*, 2001). Polyethylene oxide composites can reach 1.4×10^{-4} S cm^{-1} (Pitawala *et al.*, 2008), but only with the addition of lithium salts, 15% ceramic filler as well as 50 wt% aprotic solvents, making them unsuitable for vacuum work. It should be clear, however, that this layered all-solid-state design for Li and Li-ion batteries will allow soft X-ray studies of any cathode, anode and electrolyte material to be studied under *in situ* conditions.

Historically, soft X-ray studies have used *ex situ* samples and total electron yield (TEY) detection (Montoro *et al.*, 2000; Uchimoto *et al.*, 2001; Yoon *et al.*, 2002), in which the drain current resulting from photoemission is measured. This method suffers from background noise and a lack of data from the bulk. In partial electron yield detection, a bias grid reduces the background by rejecting low-energy electrons from other elements in the sample. PEY and TEY are surface sensitive owing to the low inelastic mean free path of electrons.

The pre-edge peak is known to correspond to molecular orbitals formed from O 2*p* and Co 3*d* orbitals, while the 540 eV peaks represent transitions from O 1*s* to molecular orbitals between O 2*p* and hybridized Co 4*sp* orbitals (de Groot *et al.*, 1989). The Co *L*-edge is split into the L_3 (780 eV) and L_2 ($\sim$795 eV) resonances, both of which correspond to transitions from Co 2*p* states to O 2*p*–Co 3*d* molecular orbitals.

In Fig. 2(*a*), oxygen *K*-edge NEXAFS data show that, in the bulk, the O 2*p*–Co 3*d* molecular orbitals are less filled than at the surface. Separately, the O 2*p*–Co 4*sp* molecular orbitals are more filled in the bulk than at the surface, leaving fewer unoccupied bound states for X-ray absorption. Fluorescence yield spectra are vulnerable to self-absorption effects in which the photons emitted from the bulk are attenuated. This tends to suppress peaks, fill in gaps between peaks, and broaden peaks. The peaks in the O *K*-edge fluorescence spectrum shown in Fig. 2 may be distorted by self-absorption, suppressing the pair of large peaks. However, the prepeak is in fact more intense in the fluorescence spectrum than in the partial electron yield spectrum; self-absorption cannot explain this difference.

Both FY and PEY O *K*-edge spectra differ considerably from the above-mentioned *ex situ* results in TEY mode in that the pre-edge peak is less intense than the post-edge peaks.

While the spectra in Fig. 2 resolve the peak at 540 eV, the feature at 536 eV appears as only a thin shoulder on the peak. To date, only one bulk sensitive *ex situ* spectrum has shown the oxygen *K*-edge in Li_xCoO_2 where x was 0.35 (Yoon *et al.*, 2004).

Yoon *et al.* (2004) found that in PEY spectra of $Li_{0.4}Mn_2O_4$ the broad peaks near 540 eV were lower in intensity compared with the 530 eV peak. Simultaneously collected FY spectra showed the 530 eV peak to have a comparable intensity with the broad peaks near 540 eV; in this work, the same surface-to-bulk trend is seen in $LiCoO_2$. Yoon *et al.* (2007) found the same trend of a reduced peak height in the bulk of $LiNi_{0.8}Co_{0.15}Al_{0.05}O_2$, yet bulk-sensitive data on $LiCoO_2$ has been missing from the literature until now.

Cobalt *L*-edge fluorescence yield data are vulnerable to self-absorption whereby the photons emitted from the bulk are partly absorbed before they escape the sample. Because absorption is nonlinear, taller peaks such as L_3 tend to be attenuated more than would L_2. This may explain the discrepancy in peak area ratios as well as the lower peak intensities in fluorescence yield data. On the other hand, deviations in the expected 2:1 peak area ratios have been observed for several transition metals and their oxides. The ratio is influenced by the 3*d* band occupancy, and is therefore sensitive to the chemical state of the transition metal ion (Leapman *et al.*, 1982). The observed differences in this ratio between the PEY and FY spectra can point to real differences in the chemical state of the transition metal ion in the surface as compared with the bulk. In future experiments, self-absorption corrections will be made by collecting FY data at multiple angles according to the analytical scheme proposed by Eisebitt *et al.* (1993).

The partial electron yield Co *L*-edge spectrum matches the total electron yield results of Yoon *et al.* (2002), but the fluorescence yield data show peak area differences. This may indicate an increased occupancy of Co 3*d* states in the bulk as compared with the surface. Fluorescent self-absorption may also play a role in reducing peak heights.

As in *ex situ* soft X-ray spectroscopy at the oxygen *K*-edge, the present samples are vulnerable to oxygen vacancies near the surface of each cathode particle. However, the vacancy concentration at room temperature will be too low to affect the spectrum.

The soft X-ray NEXAFS spectra in Fig. 3 indicate that the O local densities of state in $LiCoO_2$ changes in multiple ways upon charging the battery even before the onset of intercalation. The Co *L*-edge spectrum, meanwhile, appears not to change at all. The lack of change in cobalt agrees with charge curves (Alamgir *et al.*, 2005) showing that intercalation begins at 3.9 V or higher in $LiCoO_2$. This *in situ* measurement of the change in O local densities of state in Li-ion batteries is the first ever of its kind.

Solid-state pellet batteries described in the present work are especially useful for *in situ* surface-sensitive techniques. While this paper demonstrates the viability of direct soft X-ray spectroscopy on $LiCoO_2$, the novel cell design allows any powdered electrode material to be studied under *in situ* conditions. Also, *in situ* X-ray diffraction is feasible with some modifications. Thin film solid-state batteries also have potential for *in situ* measurements. However, thin film batteries are limited to cathode compositions which can be deposited in thin film form and heat treated while attached to a substrate, and the anode layer may be concealed. Pellet batteries can incorporate any powdered cathode, including sol–gel-derived ceramics, and the cell can be reversed for direct spectroscopic measurements on the anode.

5. Conclusions

An all-solid-state packaging-free spectroelectrochemical cell has been designed to enable simultaneous *in situ* surface-sensitive and bulk-sensitive soft X-ray absorption measurements, measurements with electron-beam sources, and mass spectroscopic measurements. The soft X-ray design allows studies complementary to those carried out at hard X-ray energies. Fluorescence yield data show, for the first time, that in $LiCoO_2$ oxygen experiences different electronic environments in the bulk as compared with the surface below the intercalation voltage. Furthermore, oxygen's chemical state changes as a function of lithium ion content. This type of information is key to understanding electrochemical reactions in $LiCoO_2$ and related battery cathode materials.

The present design allows both O *K*-edge and transition metal *L*-edge NEXAFS spectra to be obtained with a single sample at a soft X-ray synchrotron beamline. While previous *in situ* methods only measured the energy of the transition metal 4*p* orbitals, the current method measures the transition metal 3*d* orbitals and the O 2*p* orbitals, which form molecular orbitals in Li battery cathodes. *In situ* soft X-ray NEXAFS using this battery design can, therefore, detect the occupancies of all the relevant molecular orbitals in transition metal oxide intercalation cathodes.

The planetary ball mill was provided by Professor Thadhani of the Georgia Institute of Technology. Certain commercial names are mentioned in this manuscript for purposes of example and do not constitute an endorsement by the National Institute of Standards and Technology.

References

Alamgir, F. M., Ito, Y., Jain, H. & Williams, D. B. (2001). *Philos. Mag. Lett.* **81**, 213–222.
Alamgir, F. M., Strauss, E., Greenbaum, S., Whitacre, J. F., Kao, C.-C. & Neih, S. (2005). *J. Electrochem. Soc.* **152**, A845–A849.
Ceder, G., Chiang, Y.-M., Sadoway, D. R., Ayindol, M. K., Jang, Y.-I. & Huang, B. (1998). *Nature (London)*, **392**, 694–696.
Dahn, J. R., Fuller, E. W., Obrovac, M. & von Sacken, U. (1994). *Solid State Ion.* **69**, 265–270.
Deb, A., Bergmann, U., Cairns, E. J. & Cramer, S. P. (2004). *J. Synchrotron Rad.* **11**, 497–504.
Eisebitt, S., Boske, T., Rubensson, J.-E. & Eberhardt, W. (1993). *Phys. Rev. B*, **47**, 14103–14109.
Groot, F. M. F. de, Grioni, M., Fuggle, J. C., Ghijsen, J., Sawatzky, G. A. & Petersen, H. (1989). *Phys. Rev. B*, **40**, 5715–5723.
Hayashi, A., Hama, S., Morimoto, H., Tatsumisago, M. & Minami, T. (2001). *J. Am. Ceram. Soc.* **84**, 477–479.

Henke, B. L., Gullikson, E. M. & Davis, J. C. (1993). *Atom. Data Nucl. Data Tables*, **54**, 181–342.
Johnston, W. D., Heikes, R. R. & Sestrich, D. (1958). *J. Phys. Chem. Solids*, **7**, 1–13.
Koikawa, M., Gotoh, M., Ôkawa, H., Kida, S. & Kohzuma, T. (1989). *J. Chem. Soc. Dalton Trans.* pp. 1613–1616.
Leapman, R. D., Grunes, L. A. & Fejes, P. L. (1982). *Phys. Rev. B*, **26**, 614–635.
Montoro, L. A., Abbate, M. & Rosolen, J. M. (2000). *Electrochem. Solid State Lett.* **3**, 410–412.
Pitawala, H. M. J. C., Dissenanayake, M. A. K. L., Seneviratne, V. A., Mellander, B.-E. & Albinson, I. (2008). *J. Solid State Electrochem.* **12**, 783–789.
Seah, M. P. & Dench, W. A. (1979). *Surf. Interface Anal.* **1**, 2–11.
Tarascon, J.-M. & Armand, M. (2001). *Nature (London)*, **414**, 359–367.
Uchimoto, Y., Sawada, H. & Yao, T. (2001). *J. Synchrotron Rad.* **8**, 872–873.
Yoon, W.-S., Balasubramanian, M., Yang, X.-Q., Fu, Z., Fischer, D. A. & McBreen, J. (2004). *J. Electrochem. Soc.* **151**, A246–A251.
Yoon, W.-S., Chung, K., McBreen, J., Fischer, D. A. & Yang, S. (2007). *J. Power Sources*, **174**, 1015–1020.
Yoon, W.-S., Kim, K.-B., Kim, M.-G., Lee, M.-K., Shin, H.-J., Lee, J.-M., Lee, J.-S. & Yo, C.-H. (2002). *J. Phys. Chem. B*, **106**, 2526–2532.